Minutiae Verification in Fingerprint Images Using Steerable Wedge Filters

Sharat Chikkerur Venu Govindaraju
Center for Unified Biometrics and Sensors
University at Buffalo, NY, USA
(ssc5,govind)@buffalo.edu

Sharath Pankanti Ruud Bolle
IBM T. J. Watson Research Center
Hawthorne, NY, USA
(sharat,bolle)@us.ibm.com

Abstract

A majority of the existing fingerprint recognition systems are based on matching minutia features. Therefore minutiae extraction forms a very critical step and greatly influences the overall accuracy of the matching system. Poor ridge structure and processing artifacts result in missing and spurious minutia that can degrade the matching performance. We propose a novel approach based on Steerable wedge filters to eliminate false positives resulting from feature extraction. The proposed feature can also be used as a minutia detector that operates directly on the gray scale images.

1. Introduction

The fingerprint image consists of rich visual information and cues that human experts routinely utilize for fingerprint recognition. This information and redundancy present in the original data are lost during feature extraction where the entire image is reduced to a set of *minutiae* features. Minutiae represent local deviation in the flow of ridges (Figure 1). Although many different types of fingerprint features have been identified, ridge endings and bifurcation account for a majority of those features. Even this distinction is redunant. Matching algorithms usually do not distinguish between these two features as slight variation in pressure can transform a ridge ending into a bifurcation. Since most of the existing fingerprint recognition algorithms rely solely on minutiae and their structural relationship for matching [8], minutiae extraction greatly influences the overall accuracy of the matching system. Also, many of the feature extraction algorithms are sequential resulting in error propagating through each of the stages. Poor ridge structure, errors in accurately estimating the orientation field of the fingerprint and artifacts generated during fingerprint image enhancement result in the following type of errors (Figure 2)

1. *Missing minutiae*: The feature extraction algorithm fails to detect existing minutia when the minutiae is obscured by surrounding noise, scars, creases or poor ridge structures. This type of error cannot be eliminated through post processing methods.
2. *Spurious minutia*: The feature extraction algorithm falsely identifies a noisy ridge structure as a minutia. The types of errors introduced in this case strongly depend on the feature extraction process. When the feature extraction is performed using binarization and thinning, spurs, bridges, opposing minutiae, triangles, ladders are some of the structures leading to false minutiae detection [8].

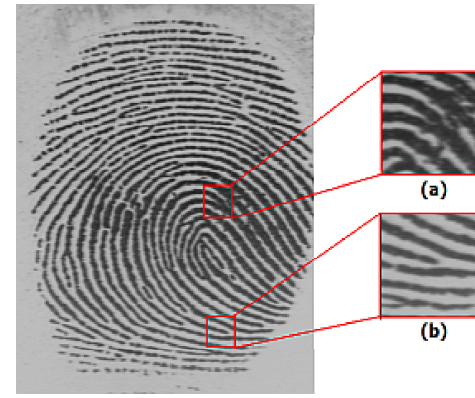

Figure 1. Fingerprint image and commonly used minutiae features (a) Bifurcation:(b)Ridge ending

Maio and Maltoni [7] proposed a feature extraction algorithm that directly operates on gray scale images alleviating many of the sources of error that are caused by binarization and thinning. The algorithm is based on tracking the ridges by following the location of the local maxima along the flow direction. However, in poor contrast or poor quality images where the local maxima cannot be reliably located, false positives are still introduced. Therefore a post-processing step is required where such spurious minutiae features are eliminated. It has been shown that feature

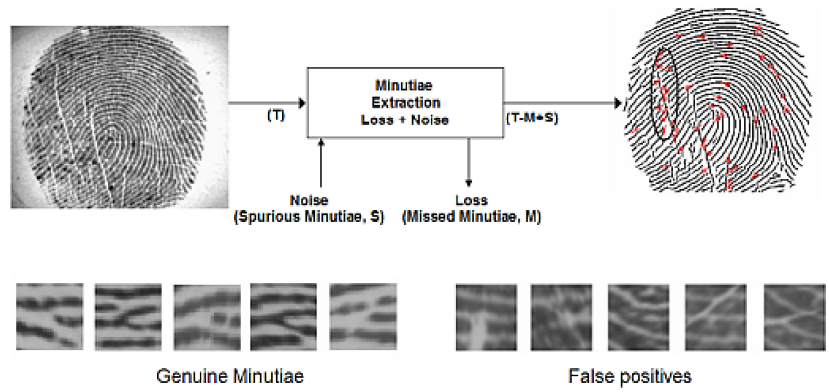

Figure 2. Errors in feature extraction. The spurious minutiae along the crease have been highlighted.

refinement can result in considerable improvement in the accuracy of a minutia based matching algorithm [10]. We propose an improved and intuitive feature set that clearly distinguishes between genuine and spurious minutia. The rest of the paper is organized as follows. Section 1.1 discusses prior related work. Section 2 describes in detail, the problem definition and the proposed approach. Results of experimental verification are presented in section 4. Conclusion and future work are discussed in section 5.

1.1. Prior related work

There have been several efforts at eliminating spurious minutia though pruning techniques. These can be broadly classified into (i)*Structural post processing* and (ii)*Gray level image based filtering*.

Structural post processing methods prune spurious minutia based on heuristics rules or ad hoc steps specific to the feature extraction algorithm. Xiao and Raafat [13] provided taxonomy of structures resulting from thinning that lead to spurious minutia and proposed heuristic rules to eliminate them. Hung [6] proposed a graph-based algorithm that exploits the duality of the ridges and bifurcation. The binarization and thinning is carried on positive and negative gray level images resulting in ridge skeleton and its complementary valley skeleton. Only the features with a corresponding counterpart are retained while eliminating the false positives. As opposed to complete elimination in pruning, Bhowmick et al. [1] propose a scoring scheme where each minutiae is assigned a score based on its reliability. The score is determined considering the topographical properties of the minutia and its neighborhood. The approach is dominantly heuristic in nature.

Gray scale based techniques use the gray scale values in the immediate neighborhood to verify the presence of a real minutia. Prabhakar et al. [9] proposed a gray scale image based approach to eliminate false minutiae. A 64x64 block surrounding a minutia is taken and is normalized with respect to orientation, brightness and variance. The block is then filtered using horizontally oriented Gabor filter [8]. The central 32x32 pixels are taken as features and the resulting 1024 dimensional vectors is used to train a supervised classifier based on Learning Vector Quantization. To compensate for the shift in minutiae location 25 different windows around each minutiae location is tested separately. The region is labeled as having minutiae if any of those 25 regions indicate the existence of a minutia. The method gives accuracy of 95% on training data and 87% accuracy on testing. However the disadvantage of this approach is that the neural network requires a 1024 length feature vector that considerably slows down the training of the network. Maio and Maltoni [3] proposed a neural network based approach for minutiae filtering relying on gray scale features. The minutia and non-minutia neighborhoods are normalized with respect to orientation and are passed to a multilayer neural network that classifies them as ridge ending, bifurcation or non-minutia. The dimensionality of the feature set is reduced by projecting the gray scale image on to a set of basis images derived using Karhunen Leove Transform. Both a positive and negative image of the neighborhood is used to exploit the duality of the ridge and bifurcation. Although the PCA improves the performance of the network, the algorithm is not very accurate when we consider a two class (minutia, vs. non-minutia) problem. Both the mentioned approaches improve the matching performance when the minutia filtering is used as a post-processing step after any of the existing feature extraction algorithms. It can be observed that existing schemes that rely solely on the image neighborhoods do not intuitively represent the nature of the problem.

2. Minutiae Verification

There is a fundamental difference in the problem of minutiae verification as defined by Prabhakar et al. [9] and Maio et al. [3] (Figure 3). In either approaches, the

neighborhoods are categorized into (i)genuine ridge endings (ii) genuine bifurcation and (iii) non-minutiae. The differences between the approaches lies in the definition of non-minutiae neighborhood. In Prabhakar et al's approach, the non-minutiae neighborhood is comprised of plain ridges where as according to Maio and Maltoni, the non-minutiae neighborhood population contains both plain ridges and actual false positives detected by their feature extraction algorithm. The problem definition as posed by Maoi and Maltoni is a more challenging one and forms the basis of our future paper, in which we have achieved significant results. In this paper, we aim to solve the problem of distinguishing non-minutia and minutia regions as defined by Prabhakar et al. .We treat both ridge endings and bifurcation uniformly since their type can get exchanged with slight variation of pressure. Also, the majority of the existing fingerprint matching algorithms does not distinguish between the minutia types during verification. Furthermore, we can also empirically show the angular response of a ridge ending and bifurcation to be equal.

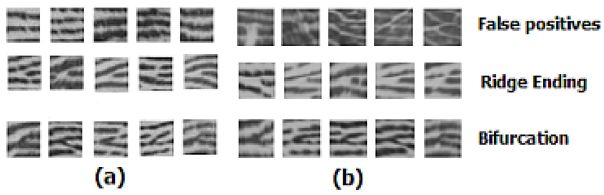

Figure 3. Minutiae neighborhood classes as proposed by (a) Prabhakar et al. and (b) Maio and Maltoni

It is evident from figure 3 that the existence of the minutiae is marked by local deviations in the ridge flow. We propose a novel feature based algorithm that intuitively represents this local deviation.

2.1. Steerable Wedge Filters

Steerable filters have been used for some time to analyze local orientation in images. Steerable filters allow us to compute the responses at different orientation as a linear combination of the image's response to a bank of basis filters. Freeman and Aldeson [5] first proposed the concept of steerable filters. They constructed the basis filters using directional derivatives of Gaussians that are either evenly or oddly symmetric. The symmetry imposes an angular periodicity of on these filter responses irrespective of the basic image structure. This introduces bimodal responses that are clearly not desirable for such tasks as junction analysis, detection or classification. Simoncelli and Farid [12] proposed a framework for steerable wedge filters that alleviate this problem. They proposed asymmetrical filters that exhibit a unimodal response. The advantage of this approach

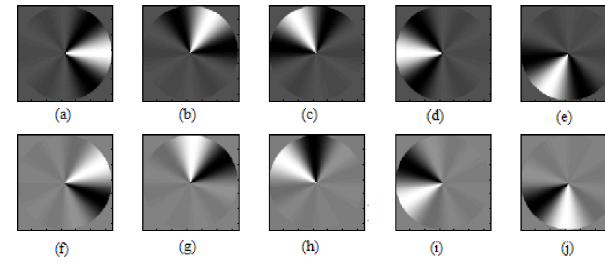

Figure 4. Steerable wedge filters for N=5 (a)-(e) evenly symmetric filters, (f)-(j)oddly symmetric filters

over using a set of oriented Gabor filter responses are as follows

1. Since the Gabor kernel is symmetric, it has a bimodal response with a period of π radians, where as the asymmetric wedge filter has a unimodal response spanning $[-\pi, \pi]$ radians.

2. Steerable filters allows us to compute the response at any arbitrary orientation as a linear sum of responses to a set of fixed basis filters. With Gabor filters, this is possible only if we perform interpolation between a set of closesly spaced filters. This would mean having a large set of oriented filters to begin with.

3. The proposed approach is more computationally efficient, since the reponse at each orientation is obtained by projecting the image onto the basis function. This only involves computing the dot products as opposed to convolving the image using a set of Gabor kernels.

A brief overview of these filters is provided for completeness. Further details are provided in [5] and [12]. The simplest example of a steerable filter is the directional derivative of radial Gaussian given by,

$$G_n^0(r,\theta) = \cos(\theta)\frac{\partial g^n(r)}{\partial r^n} \tag{1}$$

$$G_n^{\pi/2}(r,\theta) = \sin(\theta)\frac{\partial g^n(r)}{\partial r^n} \tag{2}$$

$$g(r) = e^{\frac{-r^2}{2}} \tag{3}$$

The subscript indicates the derivative order, while the superscript indicates the orientation. The filter can be synthesized in any arbitrary orientation ϕ using

$$G_n^\phi = G_n^0\cos(\phi) + G_n^{\pi/2}\sin(\phi) \tag{4}$$

The coefficients $\cos(\phi)$ and $\sin(\phi)$ are known as interpolation functions. This is the simplest case where we consider just two basis filters. To achieve steerability with filters, it is sufficient that each filter is constrained to be a

weighted sum of the first N circular harmonics [5]. The radial component of the filter can be chosen independently to be any arbitrary smooth function with compact support. The angular components of the even and odd filters are given by,

$$h_e(\phi) = \sum_{n=1}^{N} \omega_n \cos(n\phi), h_o(\phi) = \sum_{n=1}^{N} \omega_n \sin(n\phi) \quad (5)$$

The weights ω_n are chosen to maximize the impulse response $E(\phi) = h_e^2 + h_o^2$. The cost function is also weighted by ϕ to make the filter compactly supported in the angular domain. Since convolution is a linear operation, the response to any arbitrarily oriented filter may be computed using the linear combination of its responses to the basis filters.

Figure 5 shows the response of the steerable wedge filters to a typical ridge, plain ridges and false positive neighborhoods. The responses were calculated at 180 points uniformly spread in the interval [0,360] degrees. It can be observed that

- Bifurcations are marked by three dominant directions, two corresponding to the arms of the bifurcation and the third corresponding to the parallel ridge flow. In the figure, the third peak is wrapped around cyclically between 0 and 360 degrees. The response can be shown to be identical in the case of a ridge ending.
- In distinction, the non-minutia region presents bimodal response consistent with the parallel ridges in this region.
- The false positive has inconsitent peaks and dominant multiple direction.

3. Classification

It is obvious at this point that the angular response can be used to effectively distinguish the two patterns. Also, it is to be noted that if a symmetric filter was used, the response of the two arms of the bifurcation could not be resolved from the response of the plain ridges. This section presents the decision decisions and results for the classifier.

3.1. Fisher Discriminant Analysis

We investigated if it was possible to linearly separate the data. We did this by finding if there is a plane in the d-dimensional feature space that can separate the data into two distinct classes. This can be accomplished by component analysis techniques such as PCA (Principal Component Analysis) and FDA (Fisher Discriminant Analysis). We investigate FDA as it finds the line along which there is maximum separation between the two classes. It can be shown [4] that the projecting vector is given by

$$w = S_w^{-1}(m_1 - m_2) \quad (6)$$

$$S_i = \sum_{\vec{x} \in D_i} (\vec{x} - \vec{m_i})(\vec{x} - \vec{m_i})^T \quad (7)$$

$$\vec{m_i} = \frac{1}{n_i} \sum_{\vec{x} \in D_i} \vec{x} \quad (8)$$

Here represents $\vec{x}$ a d-dimensional vector (180 in our case), D_1 and D_2 represent the genuine and impostor classes and m_i represents the mean vector in the respective class. The overlap along the fisher projection (Figure 6) indicates that the classes are not linearly separable. This was further confirmed when a linear perceptron network failed to converge on the training data.

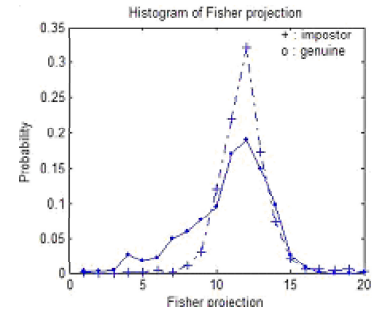

Figure 6. Large overlap in the Fisher projection of the two classes indicate the data is not linearly separable

3.2. Principal Component Analysis

The response is computed at 180 points in the interval [0,360]. In order to avoid the long training times associated with such high dimensional feature we reduce it to a lower dimensional space using PCA technique. Also, it is interesting to observe the Eigen vectors for additional insight into the problem domain. It was also found that 9 Eigen vectors are sufficient to represent the 180 dimensional feature space accurately as they contain nearly 99% of all the variance.

3.3. Neural Network

The analysis of the data through Fisher discriminant analysis and the failure of the perceptron network to converge motivated us to use a feed forward back propagation network. It is well known that a multi-layered feed forward network is capable of classifying non-linearly separated data. Furthermore we used resilient back propagation [11] algorithm to train the network. Though gradient descent

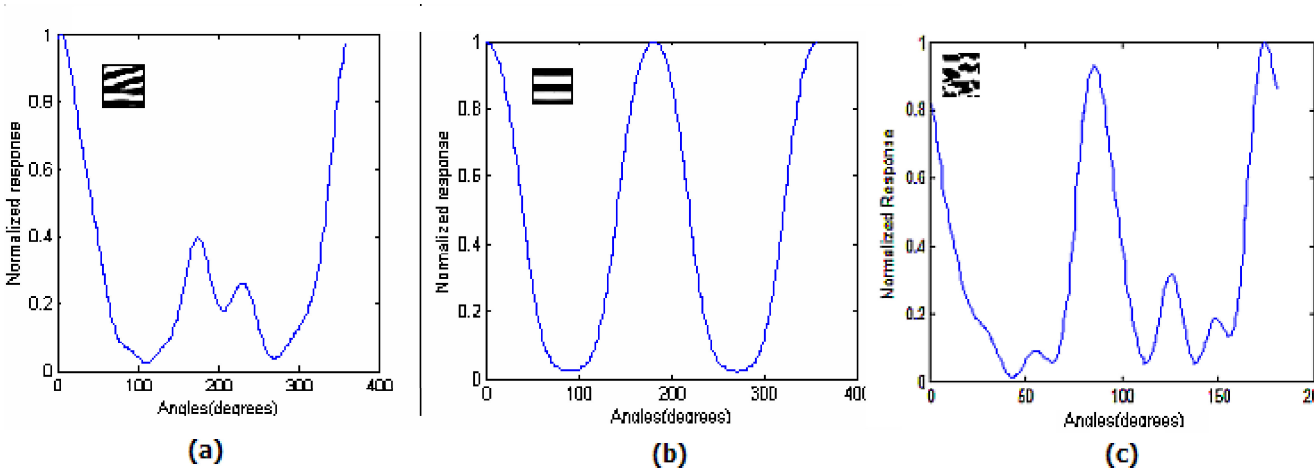

Figure 5. Response of the wedge filter to prototypical neighborhoods (a)Genuine minutia(b)Plain ridge and (c)False positive

methods are guaranteed to converge to an optimum value, the rate of convergence (gradient) steadily decreases. Furthermore this problem is also aggravated by the highly nonlinear response of the sigmoid activation function. Even when the error is very large, the weights are updated by small values as the output of the neuron is 'squashed' by the sigmoid function. The resilient back propagation algorithm by considering only the sign of the derivative for updating the weights. The change in weight is determined by a separate parameter. It was found that the resilient propagation network converges roughly more than 10 times faster than the simple back propagation algorithm and even networks includes momentum parameter and adaptive learning rates.

3.4. Support Vector Machines

Our initial experiments with the support vector machine indicated that although the accuracy of the classifier is marginally better than the neural networks, the classifier requires a very large number of support vectors to achieve the same level as classification as the neural network. It appears that for this particular problem, the neural network is able to generalize the distinctions more efficiently.

4. Experimental Evaluation

4.1. Test Data

40 randomly chosen fingerprint images from among the 2000 images in a private IBM database were used to extract genuine and impostor neighborhoods. The minutia features in the fingerprint images were manually identified using a semi-automated tool that uses the enhancement and feature extraction algorithm described in [2]. The features were visually inspected to remove outliers. The training set consisted of 1033 true minutiae 900 false minutia neighborhoods. The testing data consisted of 1000 true and 1000 false minutia neighborhoods. All the blocks are normalized with respecting to orientation and made horizontal. However there are still variations due to the valumetric differences between the blocks. To eliminate this, the blocks were then enhanced using a Fourier domain based filtering algorithm(Figure 7) also described in [2] resulting in a high contrast image that also removes the noise along the ridges.

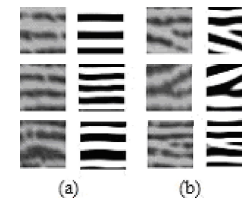

Figure 7. Normalized minutiae neighborhoods

4.2. Training

The neural network consists of a feed forward back propagation network with resilient back propagation learning algorithm. Two separate networks were trained using the same training data. The raw 180 dimensional vectors were trained using a 180-30-1 neurons network. The input to the other network consisted of 9-dimensional Eigen vector coefficients and was trained using 9-7-1 networks. The neural network was simulated using MATLAB^{TM}neural network toolbox. The network converged to a MSE of 0.013 in 2500 iterations. It is also observed that because of the resilient propagation algorithm, the PCA features do not converge significantly faster than 180-dimensional the raw feature vector.

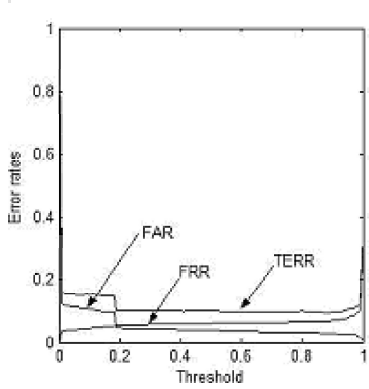

Figure 8. Error distributions for the testing data using 180 dimensional inputs

4.3. Testing

The network was tested using 1000 genuine and 1000 impostor features. The error distribution resulting from the simulation is shown in figure 8. FAR indicates the false acceptance rate (spurious minutia) and FRR indicates the false negative rate (missed minutia) TERR gives the total error due to missed and spurious minutia. The algorithm provides an accuracy(genuine accept rate) of 94.75% at the EER(Equal error rate) point. This is significantly better than the 87% accuracy mentioned by Prabhakar et al. However, we are quick to point out that any such comparison is made on the following assumption; based on the problem definition proposed by Prabhakar et al., the minutiae and plain ridges are universally defined and hence we assume that our dataset is very representative of the problem description.

5. Conclusion and Future Work

We have presented a novel feature based approach for minutiae verification in fingerprint images. Future work will involve a more objective comparison with previous work through complete implementation of Prabhakar et al. and Maio et al' work. We are also looking at the possibility of using the classifier for automatic minutia detection directly from gray scale images. Also, since the classifier gives a continuous output, the resulting value can also be used as a quality metric for the minutiae neighborhood. We are working on the possibility of including this metric during matching. Since the typically encountered fingerprint contains around 40-50 minutiae the algorithm is also computationally efficient.

References

[1] P. Bhowmick, A. Bhisnu, B. Bhattacharya, M. K. Kundu, and C. A. Murthy. Determination of minutiae scores for fingerprint image applications. In *Indian Conference on Computer Vision and Image Processing*, 2002.

[2] S. Chikkerur, C. Wu, and V. Govindaraju. A systematic approach for feature extraction in fingerprint images. In *International Conference on Biometric Authentication*, 2004.

[3] M. D. and M. D. Neural network based minutiae filtering in fingerprint images. In *14th International Conference on Pattern Recognition*, pages 1654–1658, 1998.

[4] O. R. Duda, P. E. Hart., and D. G. Stork. *Pattern Classification*. John Wiley and Sons, NY, 2001.

[5] W. Freeman and E. Aldeman. The design and use of steerable filters. *Transactions on PAMI*, 13(9):891–906, 1991.

[6] D. C. Hung. Enhancement and feature purification of fingerprint images. *Pattern Recognition*, 26(11):1661–1671, 1993.

[7] D. Maio and D. Maltoni. Direct gray scale minutia detection in fingerprints. *Transactions on PAMI*, 19(1), 1997.

[8] D. Maio, D. Maltoni, A. K. Jain, and S. Prabhakar. *Handbook of Fingerprint Recognition*. Springer Verlag, 2003.

[9] S. Prabhakar, A. Jain, and S. Pankanti. Learning fingerprint minutiae location and type. volume 36, pages 1847–1857, 2003.

[10] S. Prabhakar, A. Jain, J. Wang, S. Pankanti, and R. Bolle. Minutiae verification and classification for fingerprint matching. In *International Conference on Pattern Recognition*, volume 1, pages 25–29, 2000.

[11] M. Riedmiller and H. Braun. A direct adaptive method for faster backpropagation learning: The rprop algorithm. In *International Conference on Neural Networks*, 1993.

[12] E. P. Simoncelli and H. Farid. Steerable wedge filters for local orientation analysis. *Transactions on Image Processing*, 5(9), 1996.

[13] Q. Xiao and H. Raafat. *Combining Statistical and Structural Information for Fingerprint Image Processing Classification and Identification*, pages 335–354. World Scientific, NJ, 1991.